Modelling Recurrent Stress Drops in Porous Media

David Riley, Itai Einav, and François Guillard(✉)

The University of Sydney, Sydney, NSW 2006, Australia
francois.guillard@sydney.edu.au

Abstract. aut]Riley, Davidaut]Einav, Itaiaut]Guillard, FrançoisBrittle porous media subjected to confined compression experience rate-dependent compaction behaviour ranging from smooth stress-strain to one with recurrent abrupt drops in stress. Micromechanical investigations suggest that stress drops correlate with the collapse of the meso-scale structure. As such, we develop a novel model that qualitatively generates such behaviour. A vital feature of the model is the meso-related temperature, which characterises the fluctuating velocities at the meso-scale and, importantly, in general to all heterogeneous porous media. We assume that such temperature induces a loss of strength at the macro-scale and leads to a stress drop. Additionally, the meso-related temperature decays into micro-related (thermal) temperature, thus allowing stress to recover following a stress drop. Our model exhibits the different stress drop regimes and provides insight into the physical mechanisms required to generate these compaction patterns in brittle porous media.

Keywords: Porous media · Stress drops · Rate-dependent · Meso-scale

1 Introduction

Understanding compaction phenomena in brittle porous media are of significance for petroleum engineering, geotechnical engineering, and material science. These materials can exhibit intriguing behaviours such as rate dependence and the occurrence of recurrent stress drops. These stress drops have been observed in a variety of porous materials (e.g., sand [1], snow [2,3], cereals [4,5], and foam [6]) and typically correspond to localised compaction. However, little research has been performed to model stress drops directly, despite using continuum models to study localisation phenomena [7].

We present a continuum model that generates these recurrent stress drops while only using state variables relevant to general porous media. The key to the model's success is the meso-related temperature, which is related to the velocity fluctuations at the meso-scale and is used as a softening mechanism for the material. The meso-related temperature is first generated by macroscale dissipative processes and then feeds into thermal energy through a two-stage irreversible

E. Pasternak and A. Dyskin (Eds.): IWBDG 2022, 2023.
https://doi.org/10.1007/978-3-031-22213-9_25

process [8]. This temperature is assumed to be the physical mechanism responsible that could potentially lead to a drop in stress. The stress can recover after the softening since the meso-related temperature is dissipated into thermal temperature. Furthermore, we show that this model generates rate-dependent behaviour similar to that observed in puffed rice cereal [5] and dust [9], where increasing strain rates result in the evolution from stress drops to stress undulation with no sharp event of stress instability.

2 Model

The model developed herein depends on state variables general to all porous media. Since porous media are composed of a solid matrix, the elastic strain tensor ε^e_{ij} is a necessary state variable. We can define a bulk density ρ and solid density ρ_s since the solid material is interspersed with pores. The evolution of the bulk density ρ is determined by the mass balance equation, while a constitutive assumption gives the evolution of the solid density ρ_s. In our model, we assume that ρ_s does not change and therefore use the unstressed solid density ρ^*_s, which is constant for a given material. The introduction of these two densities naturally allows us to define a third state variable, the solid fraction $\phi = \frac{\rho}{\rho_s} \approx \frac{\rho}{\rho^*_s}$, which is critical for capturing plastic pore collapse.

The above state variables are typically applied for modelling porous media. In addition, we also include the meso-related entropy s_m to represent the mesoscopic degrees of freedom of the meso-structure [8]. The conjugate of the meso-related entropy is the meso-related temperature, which characterises the velocity fluctuations of the material at the meso-scale and is related to the thermodynamic pressure p^T in a manner that will be shown in Sect. 2.2. Our model assumes that the meso-related temperature is the phenomenological cause of macroscale softening. For example, in sand, the meso-related temperature could be generated from mechanical dissipation such as plastic pore collapse or grain breakage; alternatively, in a cellular solid, the meso-related temperature is generated from the local collapse of the solid skeleton structure. These dissipative events create new degrees of freedom that allow the local material to develop fluctuating velocities. The fluctuating velocities then decay into thermal temperature. We assume that the culmination of a potentially large number of these meso-scale regions with fluctuating velocities could induce meso-scale weakening and collapse, thus leading to macroscale softening.

Consequently, we consider the internal energy density u to be given by

$$u(\rho, \varepsilon^e_{ij}, s_m) = u^e(\rho, \varepsilon^e_{ij}) + u^m(s_m), \tag{1}$$

where u^e and u^m are the elastic energy and meso-related energy densities, respectively.

2.1 Elastic Internal Energy

We assume that the porous media can be modelled as a linear elastic material, but also include a linear dependence on density ρ. Thus, we consider the following

form for the elastic internal energy density:

$$u^e(\rho, \varepsilon^e_{ij}) = \left(\frac{\rho}{\rho^*_s}\right)\left(\frac{K}{2}\varepsilon^{e^2}_v + \frac{3}{2}G\varepsilon^{e^2}_s\right). \tag{2}$$

Here $\varepsilon^e_v = \varepsilon^e_{ii}$ is the volumetric elastic strain and $\varepsilon^e_s = \sqrt{\frac{2}{3}\varepsilon^{e\,\prime}_{ij}\varepsilon^{e\,\prime}_{ij}}$ is the triaxial elastic strain, where $\varepsilon^{e\,\prime}_{ij}$ is the deviatoric component of the elastic stress tensor. Finally, K and G are the bulk stiffness and the shear stiffness, respectively.

The elastic pressure and triaxial shear stress can then be given by

$$p^e = \frac{\partial u^e}{\partial \varepsilon^e_v} = \frac{\rho}{\rho^*_s}K\varepsilon^e_v, \tag{3}$$

$$q^e = \frac{\partial u^e}{\partial \varepsilon^e_s} = 3\frac{\rho}{\rho^*_s}G\varepsilon^e_s. \tag{4}$$

where the triaxial stress invariants can also be determined from the elastic stress tensor σ^e_{ij} by $p^e = \frac{1}{3}\sigma^e_{ii}$ and $q^e = \sqrt{\frac{3}{2}\sigma^{e\,\prime}_{ij}\sigma^{e\,\prime}_{ij}}$.

2.2 Meso-related Internal Energy, Temperature, and Thermodynamic Pressure

The meso-related internal energy was first introduced to capture the meso-related degrees of freedom for a porous media [8] and later modified [10] to the present form:

$$u^m(s_m) = \frac{s^2_m}{4}. \tag{5}$$

Through differentiation of the meso-related temperature is found to be

$$T_m = \frac{\partial u^m}{\partial s_m} = \frac{s_m}{2}. \tag{6}$$

The evolution of the meso-related temperature was derived from the corresponding entropy balance [10]. Meso-related temperature is first generated by macroscale dissipative processes and then feeds into thermal energy through a two-stage irreversible process [8], which is captured through a source term from macro-scale dissipation and sink term that depends on the current state of meso-related temperature. Furthermore, the entropy balance accounts for the advection of the meso-related temperature, which results in a Laplacian term in the evolution equation. The concepts of two-stage irreversibility and non-local interactions guide us to the form of the evolution law of the meso-related temperature, given by:

$$\partial_t T^2_m = k_m \nabla^2 T_m + \mathcal{D} - \eta T^2_m. \tag{7}$$

Here k_m is a meso-related diffusivity constant, η is a coefficient controlling the rate of energy sink from the meso-scale to the micro-scale, and

$$\mathcal{D} = p^e\dot{\varepsilon^p_v} + q^e\dot{\varepsilon^p_s}, \tag{8}$$

is the mechanical dissipation, where $\dot{\varepsilon}_v^p$ and $\dot{\varepsilon}_s^p$ are the plastic volumetric and triaxial shear strain rate invariants, respectively. For simplicity, we assume η is a constant. Note that the current paper seeks to explore only local phenomena, and thus the second gradient term in Eq. (7) will be neglected from here on.

The two-stage irreversibility concept results in a cascading of energy from meso-related temperature to the micro-related (thermal) temperature T, which results in the following form of the micro-related temperature evolution:

$$\partial_t T = k_T \nabla^2 T + \frac{\eta}{c_T \rho} T_m^2, \tag{9}$$

where k_T is the micro-related diffusivity coefficient and c_T is the specific thermal heat capacity of the porous media.

The thermodynamic pressure can be given through the following expression

$$p^T = -\left.\frac{\partial(u/\rho)}{\partial(1/\rho)}\right|_{\frac{s_m}{\rho}, \varepsilon_{ij}^e} = T_m^2. \tag{10}$$

We then recognise that the total pressure p consists of two terms in this model, $p = p^e + p^T$.

2.3 Plastic Strain Rates and Solid Fraction Evolution

Generally, many porous materials exhibit irreversible deformations with no apparent purely elastic regime, e.g., puffed rice cereals and sand. As such, we use a combination of bounding surface plasticity [11] and h^2plasticity [12] in a similar manner to [10], such that the material undergoes plastic deformations at any load. Moreover, mechanical dissipation grows instantaneously upon loading, which results in a continuous rise in the thermodynamic pressure.

From hydrodynamic derivations, it was determined that the elastic stresses are equivalent to the effective stresses [13]. Thus, we apply similar assumptions of effective stress theory that the bounding surface y and loading surface y_a depend on the elastic (effective) stresses. The bounding surface in this model is

$$y = \left(\frac{2p^e}{p_y} - 1\right)^2 + \left(\frac{2q^e}{M p_y}\right)^2 - 1 = 0, \tag{11}$$

where M is the slope of the critical state line (CSL) and p_y is the isotropic yield pressure, which depends on the solid fraction and thermodynamic pressure, as will be discussed later.

Importantly, an elliptical surface bounds both p^e and q^e, and as such it guides the plastic strains under both shear and pressure loading conditions. Furthermore, elliptical surfaces such as the one chosen for y have been used in modelling of sands [14], snow [15,16], and carbonate rock [17]. While specific shapes of a yield surface may better capture the phenomenology of particular materials, changing the shape will not negate the generation of a stress drop as long as the stress is capped in both p^e and q^e.

Now a loading surface that passes through the current stress state can be determined. We choose the loading surface to take the following form

$$y_a = \left(\frac{2p^e}{\xi p_y} - 1\right)^2 + \left(\frac{2q^e}{\xi M p_y}\right)^2 - 1 = 0, \tag{12}$$

where ξ is determined from the above equation using the current state variables. The mapping variable ξ is bounded between 0 and 1, and when $\xi = 1$ the loading surface coincides with the bounding surface. This ensures that at any non-zero stress state that $y_a = 0$ and guarantees the generation of plastic processes.

The rates of the plastic strain invariant are

$$\dot{\varepsilon_v^p} = \xi|\lambda_a|\frac{\partial y_a}{\partial p^e}, \tag{13}$$

$$\dot{\varepsilon_s^p} = \xi|\lambda_a|\frac{\partial y_a}{\partial q^e}, \tag{14}$$

where λ_a is the auxiliary non-negative plasticity multiplier. The auxiliary non-negative plasticity multiplier is solved for by the consistency condition and temporarily assuming $\xi = 1$. However, the rates of plastic strains are reduced by taking the actual value of ξ from Eq. (12). Thus, the stress state progresses away from the current loading surface for $\xi < 1$. However, if $\xi = 1$, then λ_a would keep the stress state on the loading surface which coincides with the bounding surface in this instance. Additionally, the mechanical dissipation is always non-negative since an associative flow rule was chosen and the loading surface is elliptical.

By using the conservation of mass, the evolution of solid fraction can be expressed as

$$\partial_t \phi = \phi(\dot{\varepsilon_v^p} + (1-\tau)\dot{\varepsilon_v^e}), \tag{15}$$

where τ can either be related to the solid material's Poison ratio [18] or equivalently a relative solid fraction [10]. In this paper, we assume that only plastic volumetric processes produce changes in the solid fraction ($\tau = 1$). Thus, Eq. 15 reduces to $\dot{\phi} = \phi\dot{\varepsilon_v^p}$.

Following typical conventions of modelling porous media, we take the size of the bounding surface to enlarge with increasing density but also assume that it contracts with a rise in thermodynamic pressure (kinetic softening). To account for density hardening, p_y is taken to depend nonlinearly on ϕ like that used for snow [19]. The introduction of kinetic softening is motivated by the concepts introduced in Sect. 2.2 and experimental findings in aqueous foams [20] and granular solids [21], where it was observed that stress fluctuations could induce yielding. To this end, we assume p_y declines as a function of the kinetic number $I_k = \frac{p^T}{p^e + p^T}$, which is bounded between 0 and 1 [10]. The specific form of the isotropic yield pressure is

$$p_y = \beta^* K\left((1-\phi)^{-3} - 1\right)e^{-cI_k}, \tag{16}$$

where β^* is a dimensionless positive constant, and c is a positive constant, which characterises the material sensitivity to kinetic softening. The choice of an exponential function ensures that when $p^T = 0$, the material undergoes no softening. Moreover, as $\phi \to 0$, the yield stress approaches zero, which could be further accentuated if $p^T \gg p^e$ ($I_k \to 1$). Notably, the dependence of the isotropic yield pressure on the thermodynamic pressure results in a rate-dependent plasticity model, which will be shown in Sect. 3.1.

3 Results

All simulations are oedometric tests with a constant boundary velocity V, similar to typical experimental conditions. The material parameters were assumed and chosen to be reasonable for brittle highly porous media and are used unless otherwise specified. As such, we assume that the initial solid fraction $\phi_0 = 0.25$ to represent materials such as puffed rice cereal [22], dust particles [9], and calcareous sand [23]. The shear stiffness is determined based on a chosen bulk stiffness K and Poisson's ratio ν by $G = \frac{3K(1-2\nu)}{2(1+\nu)}$. For Poisson's ratio, we assume $\nu = 0.25$, which is within the range of typical values for sand [24] and rock [25]. We assume that $M = 1.5$ is relevant for puffed rice cereals as the grains are angular and internally porous, similar to calcareous sand [26]. However, we explore the effect of different values in Sect. 3.2. Finally, we choose $c = 10$ as the value was found to generate repetitive stress drops. Table 1 summarises the chosen constants for the simulations.

Table 1. Model constants used for the simulations, unless otherwise indicated in the text.

K (kPa)	ν	β^*	M	ρ_s^* ($\frac{kg}{m^3}$)	ϕ_0	c	$\dot{\varepsilon_v}$ (s^{-1})	η (s^{-1})
10^3	0.25	$\frac{1}{10}$	1.5	600	0.25	10	0.01	10^3

3.1 Rate Dependence and Density Dependence

To relate to the dependencies observed in experiments, we explore the rate sensitivity of the model, showing that it can conceptually capture diverse rate-dependent phenomena. The simulations use a constant boundary velocity V, which is varied by several orders of magnitudes in the same manner that was done experimentally for puffed rice cereals [27]. Note that this results in an increasing instantaneous volumetric strain rate $\dot{\varepsilon_v}$ throughout the simulation.

For all scenarios in Fig. 1, the normalised axial stress initially increases with a simultaneous rise in p^T and ϕ. This steady rise continues until there is a sharp runaway of p^T (or meso-related temperature), which can be interpreted as the destruction of the meso-structure (kinetic softening). Simultaneously, there is a

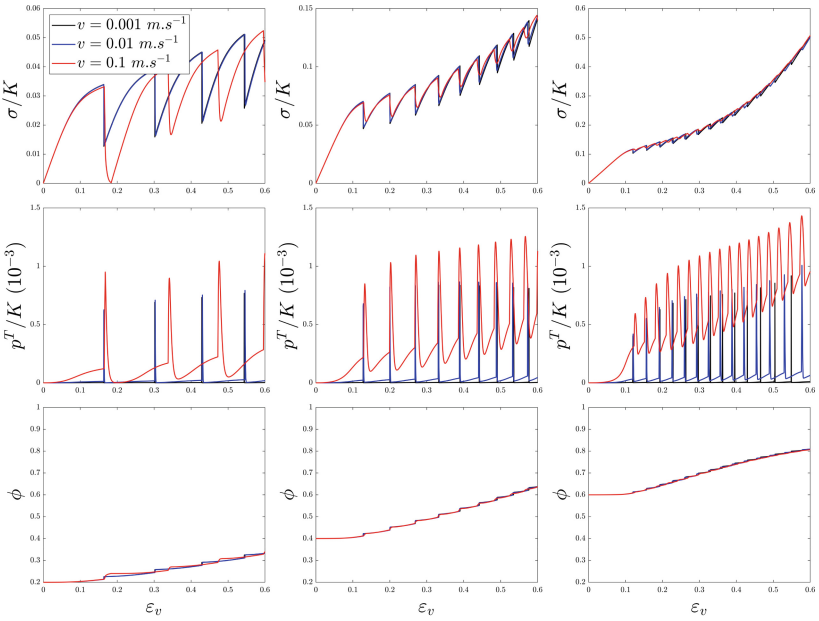

Fig. 1. The effect of strain rate and initial density on the constitutive behaviour. Panels (a–c) shows the response for three different velocities V. Here, the effects are shown for the evolution of normalised axial stress σ/K (top), normalised thermodynamic pressure p^T/K (middle), and solid fraction ϕ (bottom), for three different values of initial solid fractions, ϕ_0, all against ε_v.

sharp increase in ϕ and a rapid decline in the normalised axial stress. However, for the chosen constants, the sink term in Eq. (7) mitigates the runaway events when it becomes larger than the mechanical dissipation, which causes a decline in p^T (middle row). The decline in p^T allows for the normalised axial stress to recover. We imagine this phenomenological cycle representing competition between the destruction of the meso-structure and density hardening, which supports the development of recurrent drops in stress (top plots).

From Fig. 1, it is evident that the model exhibits rate-dependent behaviour, particularly at low initial density ($\phi_0 = 0.2$). For higher V, the thermodynamic pressure attains higher magnitudes and takes more time to dissipate into thermal temperature, as shown by the middle row of subplots. This results in a build-up of the meso-related temperature over time for the highest velocity. However, it should be noted that the model shows little change in behaviour at velocities below $V = 0.01\ \mathrm{m\,s^{-1}}$. Furthermore, the thermodynamic pressure's time-dependent relaxation results in a smoother increase in ϕ during a stress drop and generates a smoother transition from the decline in axial stress to stress recovery. Importantly, as ϕ_0 increases, the model predicts a transition from abrupt stress drops to smoother undulating drops in stress as observed exper-

imentally in dust particles and modelled for snow. Furthermore, Fig. 1 shows that under increased strain rates, the σ-ε_v curve becomes smoother, which is in line with experimental observations [5]. While the model qualitatively predicts the transition from abrupt drops in stress to a smooth σ-ε_v curve, it does not quantitatively agree with these behaviours at the appropriate initial densities or velocities. The agreement with a specific material could be improved to better capture phenomenology by using a density-dependent η or c value or a term for viscous hardening.

3.2 Critical State Slope

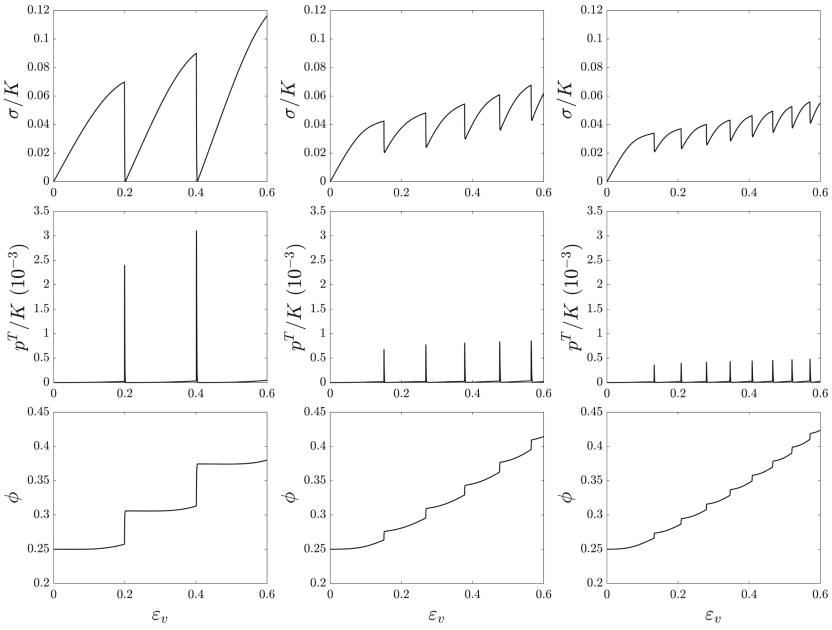

Fig. 2. The effect of the slope of the CSL on the constitutive behaviour. Panels (a-c) shows the response for three different M (in Eq. 11). Here, the effects are shown for the evolution of the normalised axial stress σ/K (top), normalised thermodynamic pressure p^T/K (middle), and solid fraction ϕ (bottom), all against ε_v.

Initially, $M = 1.5$ was assumed to be potentially reasonable for puffed rice cereals and calcareous sand, but now we explore the effect on the constitutive response. It is important to explore this as some porous materials could be relatively spherical and smooth, which leads to a lower M, such as glass beads, and still generate stress drops [7]. In granular materials, M is correlated with the internal friction angle, and thus one might expect that it could impact the material's

susceptibility to the destruction of the meso-scale. Thus, M was varied from 1 to 2 to identify its impact on the model response. In this section we prescribe $V = 0.01\ \mathrm{m\,s^{-1}}$.

From Fig. 2, the decrease of axial stress during an axial stress drop is significantly larger and occurs less frequently for a low M, which matches experimental observations in glass beads [9]. These substantial drops in stress correspond to a significant increase in solid fraction ϕ and thermodynamic pressure. We interpret this as a result of low internal friction, resulting in more pronounced destruction of the meso-scale structure from velocity fluctuations at the meso-scale (meso-related temperature). As M increases, the stress drop magnitudes decrease, where in granular media, this phenomenology could be a result of higher internal friction that prohibits the destruction of the meso-scale. Moreover, these drops increase in frequency and result in a higher amount of plastic pore collapse (bottom plots).

4 Conclusions

Brittle porous media have been shown to exhibit fascinating rate-dependent compaction patterns. We develop a constitutive model, which generates recurrent abrupt stress drops and reproduces the rate-dependent transitions in compaction as observed experimentally. The critical component to the generation of these features is the introduction of the meso-related temperature, which captures in a phenomenological manner the entropy production associated with meso-scale velocity fluctuations. This temperature is assumed to destroy the meso-scale structure in heterogeneous porous media. Thus, we use the meso-related temperature to induce macroscale kinetic softening.

The occurrence and frequency of the abrupt recurrent stress drops are dependent on the competition between the destruction of the meso-structure (kinetic softening) and density hardening. Moreover, internal friction within the material is accounted for, which can moderate the magnitude of stress drops. Thus, the model can reproduce the behaviours of materials ranging from glass beads to cereals. Additionally, the time-dependent nature of sinking meso-related temperature to micro-related temperature results in rate dependence similar to that observed in puffed rice cereal [27] and dust particles [9], where the stress drops transition from abrupt to undulating with a reduced magnitude. However, these results occurred at different initial densities than those expected from experimental results. A better quantitative agreement could be achieved by using state-dependent functions for c or η or including a viscous hardening term, but these are left for future research.

While this model was developed to be general for all porous media that undergo pore collapse and density hardening, it could be enhanced to capture specific material's behaviour. The extension of the model to specific materials should be possible as the model's behaviour emerges from state variables that are useful in describing all porous media. For example, in the case of sand, the combination of breakage and pore collapse contributes to plastic dissipative processes

and could be accounted for by combining this model with breakage mechanics [18]. Alternatively, the model could be tuned to reproduce the behaviours of metallic foam by applying a yield surface shape known to produce behaviours associated with such materials.

References

1. Michlmayr, G., Cohen, D., Or, D.: Shear-induced force fluctuations and acoustic emissions in granular material. J. Geophys. Res.: Solid Earth **118**(12), 6086–6098 (2013)
2. Yosida, Z., Oura, H., Kuroiwa, D., Huzioka, T., Kojima, K., Kinosita, S.: Physical studies on deposited snow. IV.; mechanical properties (3). Contrib. Inst. Low Temperature Sci. **13**, 55–100 (1958)
3. Löwe, H., Zaiser, M., Mösinger, S., Schleef, S.: Snow mechanics near the ductile-brittle transition: compressive stick-slip and snow microquakes. Geophys. Res. Lett. **47**(4), e2019GL085491 (2020)
4. Valdes, J.R., Fernandes, F.L., Einav, I.: Periodic propagation of localized compaction in a brittle granular material. Granular Matter **14**(1), 71–76 (2012)
5. Valdes, J.R., Guillard, F., Einav, I.: Evidence that strain-rate softening is not necessary for material instability patterns. Phys. Rev. Lett. **119**(11), 118004 (2017)
6. Papka, S.D., Kyriakides, S.: In-plane crushing of a polycarbonate honeycomb. Int. J. Solids Struct. **35**(3–4), 239–267 (1998)
7. Kuhn, M.R., Daouadji, A.: Stress fluctuations during monotonic loading of dense three-dimensional granular materials. Granular Matter **21**(1), 1–14 (2019). https://doi.org/10.1007/s10035-018-0861-7
8. Jiang, Y., Liu, M.: Granular solid hydrodynamics. Granular Matter **11**(3), 139–156 (2009)
9. Pacheco-Vázquez, F., Omura, T., Katsuragi, H.: Undulating compression and multistage relaxation in a granular column consisting of dust particles or glass beads. Phys. Rev. Res. **3**(1), 013190 (2021)
10. Alaei, E., Marks, B., Einav, I.: A hydrodynamic-plastic formulation for modelling sand using a minimal set of parameters. J. Mech. Phys. Solids **151**, 104388 (2021)
11. Dafalias, Y.F.: Bounding surface plasticity. I: Mathematical foundation and hypoplasticity. J. Eng. Mech. **112**(9), 966–987 (1986)
12. Einav, I.: The unification of hypo-plastic and elasto-plastic theories. Int. J. Solids Struct. **49**(11–12), 1305–1315 (2012)
13. Einav, I., Liu, M.: Hydrodynamic derivation of the work input to fully and partially saturated soils. J. Mech. Phys. Solids **110**, 205–217 (2018)
14. Roscoe, K., Burland, J.: On the generalized stress-strain behaviour of wet clay. In: Engineering Plasticity, pp. 535–609 (1968)
15. Meschke, G., Liu, C., Mang, H.A.: Large strain finite-element analysis of snow. J. Eng. Mech. **122**(7), 591–602 (1996)
16. Gaume, J., Gast, T., Teran, J., Van Herwijnen, A., Jiang, C.: Dynamic anticrack propagation in snow. Nat. Commun. **9**(1), 1–10 (2018)
17. Abdallah, Y., Sulem, J., Stefanou, I.: Compaction banding in high-porosity carbonate rocks: 2. A gradient-dependent plasticity model. J. Geophys. Res.: Solid Earth **125**(12), e2020JB020610 (2020)
18. Tengattini, A., Das, A., Einav, I.: A constitutive modelling framework predicting critical state in sand undergoing crushing and dilation. Géotechnique **66**(9), 695–710 (2016)

19. Barraclough, T.W., Blackford, J.R., Liebenstein, S., Sandfeld, S., Stratford, T.J., Weinländer, G., Zaiser, M.: Propagating compaction bands in confined compression of snow. Nat. Phys. **13**(3), 272–275 (2017)
20. Debregeas, G., Tabuteau, H., Di Meglio, J.M.: Deformation and flow of a two-dimensional foam under continuous shear. Phys. Rev. Lett. **87**(17), 178305 (2001)
21. Pouliquen, O., Forterre, Y., Le Dizes, S.: Slow dense granular flows as a self-induced process. Adv. Complex Syst. **4**(04), 441–450 (2001)
22. Einav, I., Guillard, F.: Tracking time with ricequakes in partially soaked brittle porous media. Sci. Adv. **4**(10), eaat6961 (2018)
23. Lv, Y., Wang, Y., Zuo, D.: Effects of particle size on dynamic constitutive relation and energy absorption of calcareous sand. Powder Technol. **356**, 21–30 (2019)
24. Coduto, D.P., Kitch, W.A., Yeung, M.C.R.: Foundation Design: Principles and Practices, vol. 2. Prentice Hall, USA (2001)
25. Gercek, H.: Poisson's ratio values for rocks. Int. J. Rock Mechan. Mining Sci. **44**(1), 1–13 (2007)
26. Zhang, J., Luo, M.: Dilatancy and critical state of calcareous sand incorporating particle breakage. Int. J. Geomech. **20**(4), 04020030 (2020)
27. Guillard, F., Golshan, P., Shen, L., Valdes, J.R., Einav, I.: Dynamic patterns of compaction in brittle porous media. Nat. Phys. **11**(10), 835–838 (2015)